

Journal of Biomedical Optics

SPIEDigitalLibrary.org/jbo

Noninvasive *in vivo* optical assessment of blood brain barrier permeability and brain tissue drug deposition in rabbits

Aysegul Ergin
Mei Wang
Jane Zhang
Irving Bigio
Shailendra Joshi

Noninvasive *in vivo* optical assessment of blood brain barrier permeability and brain tissue drug deposition in rabbits

Aysegul Ergin,^a Mei Wang,^b Jane Zhang,^a Irving Bigio,^c and Shailendra Joshi^b

^aBoston University, Department of Biomedical Engineering, 44 Cummington Street, Boston, Massachusetts 02215

^bCollege of Physicians and Surgeons of Columbia University, Department of Anesthesiology, P&S Box 46, 630 West 168th Street, New York, New York 10032

^cBoston University, Department of Biomedical Engineering, Electrical Engineering, Physics and Medicine, 44 Cummington Street, Boston, Massachusetts 02215

Abstract. Osmotic disruption of the blood brain barrier (BBB) by intraarterial mannitol injection is sometimes the key step for the delivery of chemotherapeutic drugs to brain tissue. BBB disruption (BBBD) with mannitol, however, can be highly variable and could impact local drug deposition. We use optical pharmacokinetics, which is based on diffuse reflectance spectroscopy, to track *in vivo* brain tissue concentrations of indocyanine green (ICG), an optical reporter used to monitor BBBD, and mitoxantrone (MTX), a chemotherapy agent that does not deposit in brain tissue without BBBD, in anesthetized New Zealand white rabbits. Results show a significant increase in the tissue ICG concentrations with BBBD, and our method is able to track the animal-to-animal variation in tissue ICG and MTX concentrations after BBBD. The tissue concentrations of MTX increase with barrier disruption and are found to be correlated to the degree of disruption, as assessed by the ICG prior to the injection of the drug. These findings should encourage the development of tracers and optical methods capable of quantifying the degree of BBBD, with the goal of improving drug delivery. © 2012 Society of Photo-Optical Instrumentation Engineers (SPIE). [DOI: 10.1117/1.JBO.17.5.057008]

Keywords: diagnostic optical spectroscopy; blood brain barrier disruption; optical pharmacokinetics; mitoxantrone; indocyanine green; chemotherapy.

Paper 11447 received Aug. 18, 2011; revised manuscript received Feb. 28, 2012; accepted for publication Mar. 1, 2012; published online May 21, 2012.

1 Introduction

Timely and effective drug delivery to brain tissue remains a major hurdle to the treatment of brain tumors, partly due to the blood brain barrier (BBB), which imposes a significant restriction on drug delivery.^{1,2} It is generally believed that disruption of the barrier would increase uptake of chemotherapeutic drugs. To that end, intraarterial (IA) mannitol has been the main method of barrier disruption in the last three decades. However, osmotic disruption of the BBB is affected by several factors and can vary significantly among mannitol treatments. The value of both IA drug delivery and osmotic disruption of BBB remains largely unproven in rigorous clinical trials. In theory, IA delivery of drugs can achieve therapeutic concentrations in brain tissue almost instantaneously and at a fraction of typical systemic doses.³ However, the pharmacokinetics of IA drug delivery are complex and ill understood.^{3,4} The rapid changes in drug concentrations that follow IA injections are beyond the time resolution of conventional tissue biopsy or microdialysis methods. Under these circumstances, the ability to track brain tissue concentrations of drugs and tracers in virtual-real time by a noninvasive and nondestructive optical pharmacokinetics (OP) method is particularly attractive.^{5,6}

In earlier studies, we demonstrated the feasibility of tracking brain tissue concentrations of mitoxantrone (MTX), an anticancer drug with potential for treating malignant gliomas, by using the OP method.^{7,8} Also, Kanick et al. reported that they can detect absorbance attributable to motexafin gadolinium, another anti-cancer agent, in mouse tissues *in vivo* and *in situ* using the OP method.⁹ We further showed that the barrier disruption could be detected by measuring tissue concentrations of indocyanine green (ICG), a widely used, Food and Drug Administration (FDA) approved, water soluble dye injected intravenously.¹⁰ In the present study, we use IA injection of ICG to assess BBB permeability after mannitol injection, and we use the OP method to determine the tissue concentrations of MTX. Preliminary reports suggest that MTX delivery into brain tissue can be enhanced by BBB disruption (BBBD).⁷ In parallel studies, we had observed that BBBD in rabbits with IA mannitol was highly variable.^{11,12} Similar variability in the degree of BBBD has also been reported in human subjects.¹³ Such variability could have a very significant impact on the delivery of chemotherapeutic drugs that require BBBD. In clinical settings, BBBD by mannitol is often assessed after the delivery of drugs.^{13,14} Positron emission tomography (PET) and magnetic resonance imaging (MRI) have been demonstrated as real-time monitors of BBBD;^{15,16} these methods, however, are cumbersome and expensive. Given the lower cost, real-time assessment of BBB permeability by optical means could

Address all correspondence to: Shailendra Joshi, College of Physicians and Surgeons of Columbia University, Department of Anesthesiology, P&S Box 46, 630 West 168th Street, New York 10032. Tel: +212 305 0021; Fax: +2123058287; E-mail: sj121@columbia.edu

ultimately improve clinical drug delivery. In the present report, we show the feasibility of real-time monitoring of BBB permeability and local drug concentrations using the OP method with our rabbit model.

2 Material and Methods

2.1 Animal Preparation

After approval of the investigation protocol by the Institutional Animal Care and Use Committee of Columbia University, studies were conducted on 16 New Zealand white rabbits 1.5 to 2 kg in weight. The large size of their skull is convenient for implanting a laser Doppler (LD) probe and placing the OP probe. Laser Doppler flow (LDF) is used as a measure of cerebral blood flow (CBF), and the OP probe is used to collect spectral data for dye or drug measurements. Rabbits have a primate-like separation of internal and external carotid irrigations; therefore, they are well suited for IA drug delivery experiments.

2.2 Optical Pharmacokinetics

The method of OP is a version of diffuse reflectance spectroscopy, which enables the noninvasive real-time measurement of drug concentrations *in situ*. A schematic of the setup is shown in Fig. 1. The OP method determines drug concentrations by measurement of the wavelength-dependent optical absorption coefficient of the tissue, and it can be used for drugs that have an absorption band within the wavelength range from visible to near-infrared (450 to 950 nm). The underlying optical-physics principles for the OP method have been described in detail in earlier publications by Bigio and collaborators, who reported the preclinical measurements of chemotherapeutic drug concentrations in animal models in the peripheral tissues.^{5,6} It was shown that, for an appropriate range of fiber separations between light delivery and collection fibers, the path length of the collected photons is insensitive to variations in scattering properties for the range of scattering parameters typically found in tissue. As employed in these studies, the fiber separation is 2 mm, and the depth of sensitivity is 2 to 3 mm.¹⁷

An optical fiber probe, comprising separate illumination and collection fibers, was placed in gentle contact with the tissue surface during measurement.^{5-9,18} Although the device can sample light backscattered from the sub-surface tissue as

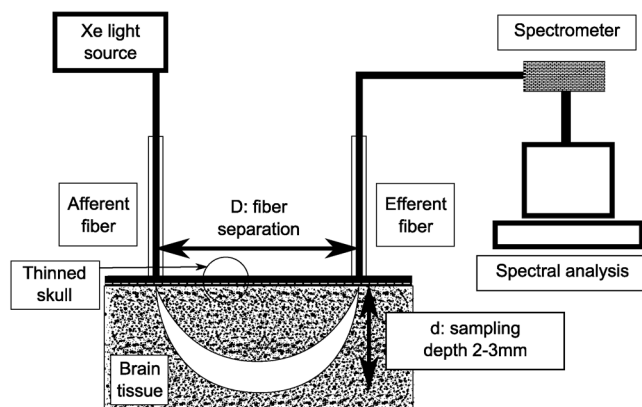


Fig. 1 A schematic of the optical pharmacokinetics device that uses a variation of diffuse reflectance spectroscopy for measuring concentrations of absorbers in turbid media.

frequently as every 50 ms, for the current study, the samples were acquired every 500 ms to 5 s. Twelve baseline measurements were acquired every 5 s before injection of ICG and MTX. The optical data were acquired at multiple repetition rates after ICG and MTX injections. At the start of IA ICG and MTX injection, 300 measurements were acquired at 750 ms intervals to record the rapid first-pass kinetics of the tracers through brain tissue. An additional 300 measurements were collected every 2.5 s during MTX injection to record slower changes over 30 min. Optical determination of ICG and MTX concentrations was done by using a modified Beer's law, as previously described.⁵⁻⁸ All computational analyses were completed using Matlab® (The MathWorks, Inc.) software.

2.3 Optical Determination of Tissue ICG and MTX Concentrations

One of the challenges in this study was to determine the concentration of ICG in the brain tissue. The ICG absorption spectrum is affected by the solvent and the dye concentration. Furthermore, binding to blood plasma proteins also causes changes in the absorption spectrum of ICG^{19,20} as shown in Fig. 2. We observed this spectral instability in the data collected during this study (Fig. 3).

In the analysis, collected spectral data were analyzed first by taking the ratio of each spectrum after dye or drug injection to the spectrum taken before dye or drug addition. Later, the negative log of this ratio was used to fit Eq. (1) to estimate the concentration of ICG and MTX in the brain tissue at each time point during the experiment.

$$-\log\left(\frac{I_t}{I_0}\right) = B(\lambda) + \Delta(\mu_a)L(\mu_a). \quad (1)$$

In this equation, I_0 and I_t are measurements before and anytime after the dye injection, respectively. $B(\lambda)$ accounts for the baseline shift during measurements, and it is wavelength dependent, as expressed in Eq. (2). $\Delta\mu_a$ is the change in the tissue absorption coefficient, and $L(\mu_a)$ accounts for the absorption dependent path length. Although $L(\mu_a)$ is insensitive to changes in scattering for certain fiber separations, it still depends on the absorption, especially for *in vivo* applications where the hemoglobin absorbs very strongly. In previous studies, it was found that Eq. (3) can describe the dependence of path length on absorption. In Eq. (3), x_0 , x_1 , and x_2 are calibration coefficients specific to the probe geometry, which are obtained by taking measurements on a phantom with known optical properties.⁶ For this study, the values were determined from measurements in 1% intralipid phantom, which yields a reduced scattering coefficient of approximately 10 cm^{-1} , a typical value for tissue. The absorption coefficient was $\sim 0.3 \text{ cm}^{-1}$ at 700 nm, which is in the range of the absorption in tissue at that wavelength.

$B(\lambda)$, $L(\mu_a)$ and $\Delta\mu_a$ are defined as

$$B(\lambda) = c_0 + c_1\lambda + c_2\lambda^2, \quad (2)$$

$$L(\mu_a) = x_0 + x_1 \exp(-x_2\mu_a), \quad (3)$$

$$\Delta\mu_a = [\Delta C_{\text{HbO}(t)}\epsilon_{\text{HbO}(\lambda)} + \Delta C_{\text{Hb}(t)}\epsilon_{\text{Hb}(\lambda)} + C_{\text{drug}(t)}\epsilon_{\text{drug}(\lambda)}]. \quad (4)$$

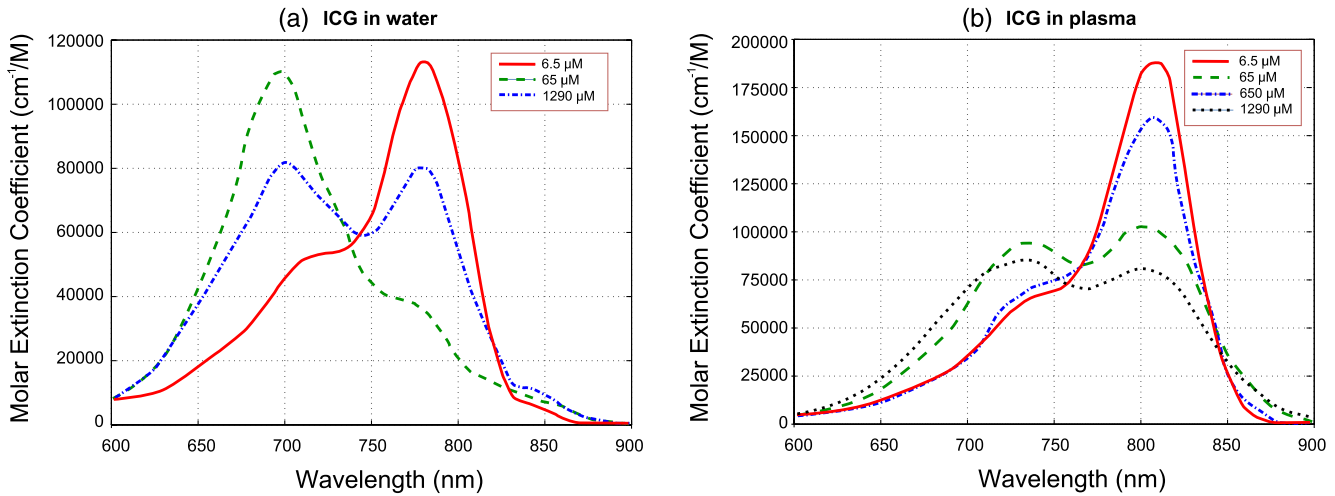


Fig. 2 The absorption spectra of ICG (a) in water and (b) in plasma. The data in these graphs are digitized from Landsman et al.¹⁹ and replotted as wavelength versus molar extinction coefficient by Scott Prah, Oregon Medical Laser Center.²⁰

In Eq. (4), the change in concentrations of oxyhemoglobin (HbO) and deoxyhemoglobin (Hb) are represented by $\Delta C_{HbO(t)}$ and $C_{Hb(t)}$. The concentration of the dye or drug is represented by $C_{drug(t)}$, and the extinction coefficients of HbO, Hb, and the dye or drug are given by $\epsilon_{HbO(\lambda)}$, $\epsilon_{Hb(\lambda)}$, and $\epsilon_{drug(\lambda)}$, respectively. Fitting of the collected spectral data to Eq. (1) required the use of absorption spectra of Hb, HbO, ICG, and MTX.

During the IA injection of ICG, we observed a transient decrease in CBF, which was due to a momentary displacement of the blood by the ICG solution. During this transient time, ICG was found free, unbound to plasma proteins. For this time point of injection, we used the spectrum of ICG in water (1290 μM) measured by Landsman et al.,¹⁹ as the absorption spectrum

in the fitting algorithm to quantify ICG concentration. As the injection ended, ICG became bound to plasma proteins, as it was rapidly diluted by the blood. We observed that the ICG spectrum quickly stabilized after the bolus injection ended and did not show a spectral change for the rest of the experiment. For these after-injection time points, the protein-bound ICG spectrum in plasma (65 μM) was used in the fitting algorithm. The first couple of spectra collected by OP during the ICG injection can be seen in Fig. 3. We observed similar transitional spectral changes in all animal data collected by OP. Two chosen spectra we used, fit well to the absorption spectra collected during OP measurements. Also, the chosen spectra had the closest concentration values to the ICG dose used in this study.

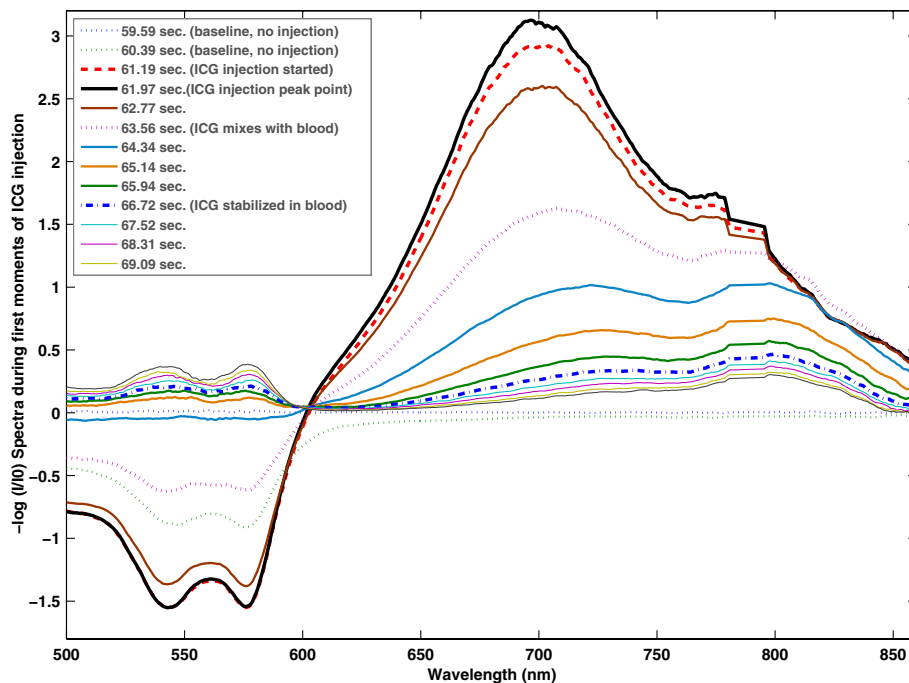


Fig. 3 Selected $-\log(I/I_0)$ raw spectra collected by OP during the intraarterial injection of ICG. The spectra change during the first few moments of the injection as the ICG is diluted by blood.

Choosing a different absorption spectrum of ICG for specific time points of the injection helped to minimize the quantification errors that might be caused by the spectral instability of this dye.

The optical absorption spectrum of MTX is distinct from that of Hb and of HbO. Therefore, it is well suited for tissue concentration measurements by the OP method. The absorption spectrum of MTX (13.5 μm in saline) was measured with a spectrophotometer and used in the fitting algorithm (Fig. 4). MTX is known to bind to DNA. Intercalation with DNA is known to cause a 15 to 20 nm red shift of the absorption peaks.⁶ The absorption spectrum is also affected by the solvent.²¹ In this study, we carefully checked the absorption band of MTX in the spectral data collected by OP, but we did not observe any spectral shift due to DNA intercalation.

2.4 Surgical Preparation

After placement of an intravenous (IV) line, the animals were anesthetized with 0.2 to 0.5 ml boluses of intravenous 1% propofol (Diprivan®, Astra Zeneca, Wilmington, DL). Subsequently, the animals were ventilated through a tracheotomy, using a Harvard ventilator. The ventilator rate was adjusted to produce a stable mixed end-tidal CO_2 of 15 to 20 mm Hg, corresponding to an effective end-tidal pressure of 30 to 40 mm Hg. Anesthesia was maintained with continuous propofol infusion at a rate of 20 to 30 mg/h and supplemental intramuscular ketamine. An esophageal temperature probe monitored the core temperature of the animal. The animal was kept warm using a servo controlled electrical mattress. The femoral and common carotid arteries were cannulated, and the internal carotid artery was carefully isolated from other branches.²²

Thereafter, the animals were placed prone in a stereotactic frame for the placement of electroencephalographic leads, LD, and OP probes. Through a midline incision, the periosteum of the skull was exposed. Electroencephalographic leads were secured to the skull with 1.5 mm stainless steel screws. The skull was gently milled down, such that cerebral arteries could be seen through the inner table, in effect serving like a cranial window. The cranial vault integrity was not internally compromised. Thinning the skull was an alternate approach

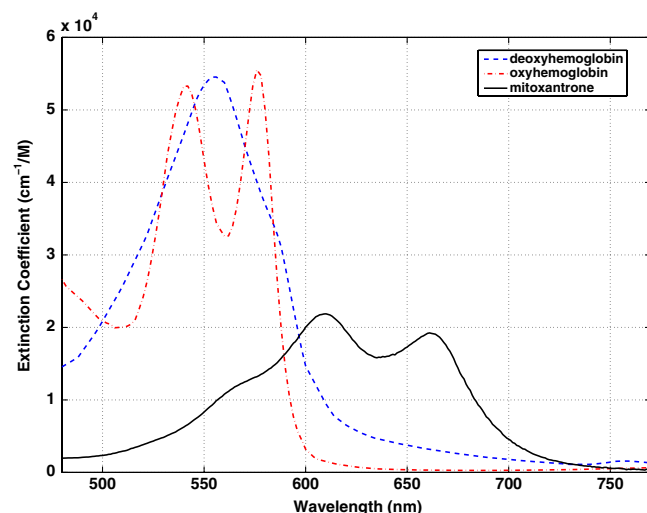


Fig. 4 Spectra of oxyhemoglobin, deoxyhemoglobin, and mitoxantrone (13.5 μm in saline).

to implanting glass windows. This approach minimized chances of brain injury. Based on microscopic imaging, we estimated that the thickness of the skull was in the range of 200 to 500 microns. The LD probes were secured in plastic retainers that were glued to the skull. The OP probe was placed with a micro-manipulator so that the probe tip was in gentle contact with the thinned skull over the brain, lightly flattening the thinned bone. The OP probe, which has an external diameter of 3 mm, was placed over a relatively avascular region of the frontal cortex, away from the midline. Most vessels in this region were fairly small, and they can be clearly seen through the thinned skull. The OP probe was placed in a region away from these vessels. Furthermore, in this region of the rabbit brain, the optical signals caused by brain pulsations were minimal, and the probe remained stable even during prolonged use. After the probe placement, the OP signal was checked to confirm that there was not strong absorption in the hemoglobin region of the spectrum around 550 nm. Meticulous care was taken to avoid bleeding. Paper drains were placed around the surgical site to divert blood away from the site of OP measurements to avoid any contamination of the measurement site during the experiments. Bone wax was used to seal the edges.

2.5 Tracer and Drug Doses and Delivery

ICG was selected as the optical tracer because it has an absorption spectrum that is distinct from those of oxy- and deoxyhemoglobin and is FDA approved for human diagnostic applications. A 0.1% solution (1 mg/ml) of ICG (Cardio Green, Sigma Aldridge Co., St. Louis, MO) was prepared in sterile water immediately prior to use. The pH of the 0.1% ICG solution was 7.34. In a preliminary animal study, we determined that a 1 mg dose of ICG could be robustly measured by the OP method, and it would be rapidly cleared after IA administration (Fig. 5). One millilitres of ICG was injected by solenoid controlled pneumatic pump over 2 s. MTX, a water soluble chemotherapy agent, was selected as the drug, and 3 ml of 0.1% (1 mg/ml) of MTX in normal saline (Sigma Aldridge Co., St. Louis, MO) was injected with an IVAC syringe pump in bolus mode over 30 s. Mannitol, warmed to 37°C and filtered through a 0.2 micrometer filter, was hand injected (25%,

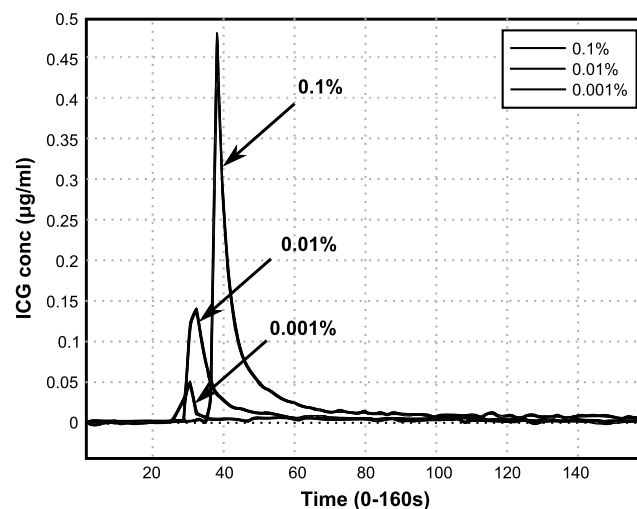


Fig. 5 Dose response to intraarterial injection of increasing concentrations of ICG without BBB disruption. Injection times are at $t = 25$ s, $t = 30$ s, and $t = 35$ s for doses 0.001%, 0.01%, and 0.1%, respectively.

0.25 ml/kg/s for 30 s) after it was determined that mechanical pumps were unable to reliably administer the IA dose of mannitol required for this experiment.¹¹ In the control group, equivalent intravenous volume of saline was injected instead of mannitol over the same time period.

2.6 Experimental Design

The experimental protocol is shown in Fig. 6. Animals that were randomized to the control group received intravenous saline bolus over 30 s, while the treatment group received IA injection of mannitol. Each group had eight animals. There are reports of intravenous mannitol resulting in BBBB.²³ Therefore, intravenous saline was used as the control to simulate volume loading and avoid any inadvertent disruption of BBB. In order to increase the transit time, a small bolus of 10 mg adenosine and 10 mg esmolol were injected to transiently decrease transiently CBF during mannitol injection. Adenosine and esmolol are known to induce hypoperfusion and reduction in blood flow. Mannitol acts by dehydrating the endothelial cells, and the transient hypoperfusion increases the osmotic stress.¹¹ IA ICG bolus was injected 5 min after intravenous saline or mannitol injection. Another 5 min later, IA MTX was injected 5 min. after IA ICG injection.

2.7 Data Collection and Analysis

ICG and MTX concentration-time curves were generated using the collected OP data and the parameters that were analyzed included baseline, peak concentration, final brain tissue concentration 5 min after ICG injection (30 min after MTX injection), and area under the concentration-time curve (AUC). AUC is the area under the time-concentration curve plotted using the ICG or MTX concentration values at each time point, as measured by the OP method, for the duration of the experiment. The definite integral was used to find the area, and it represents the amount of ICG or MTX uptake by the brain tissue measured by OP.

Bilateral hemispheric electrocerebral and electrocardiographic activities, mean femoral arterial (MAP) pressure, heart rate (HR), and CBF were recorded using LD; esophageal and tympanic temperatures, pulse oxygen saturation (SaO₂), and the ventilatory parameters were recorded by the Mac-Lab data (AD Instruments) collection system. The physiological data for analysis included HR, MAP, CBF, core temperature, respiratory rate, and end-tidal carbon-dioxide tension (ETCO₂).

2.8 Statistical Data Analysis

The data were analyzed by factorial and repeated measures ANOVA methods. For single factor comparisons, e.g., control

versus mannitol treated group, a *p* value of 0.05 was considered significant. The Bonferroni-Dunn test was used to correct for multiple comparisons among the hemodynamic parameters at different stages of ICG and MTX injections, as shown in the tables. A more stringent *p* value of 0.005 was considered significant for multiple comparisons of hemodynamic data. To determine the effects of BBBB on the uptake of MTX, simple linear correlation was used to determine the relationships between MTX and ICG concentrations.

3 Results

The study was conducted on 16 New Zealand white rabbits with comparable mean weights of 1.8 ± 0.2 and 1.7 ± 0.1 kg in the control versus the mannitol groups.

3.1 Uptake of ICG and MTX

Baseline ICG concentration was determined using the OP data collected 1 to 2 min just before any injection was made to the animal. It was effectively zero (within the noise level of $\sim 2 \times 10^{-6}$ mg/ml) and increased to a peak value of $3 \times 10^{-3} \pm 1 \times 10^{-3}$ mg/ml within 5 to 10 s ($n = 8$, $p < 0.001$). In the control group, there was no difference between the baseline and end concentration of ICG. Both were effectively zero within noise. The end concentrations of ICG were significantly higher in the mannitol group compared to the control group: $1 \times 10^{-3} \pm 3.08 \times 10^{-4}$ versus $6.83 \times 10^{-5} \pm 3.39 \times 10^{-5}$ mg/ml, respectively ($n = 8$, $p < 0.0014$) [Fig. 7(a)]. In the case of MTX, a strong trend for higher peak concentrations was encountered after mannitol injection compared to the control group: $5 \times 10^{-3} \pm 3 \times 10^{-3}$ versus $1 \times 10^{-2} \pm 6 \times 10^{-3}$ mg/ml, respectively ($n = 8$, $p = 0.0727$) [Fig. 7(b)]. It should be noted that the blood flow when compared with the start of the experiment (saline baseline) was lower in the mannitol group prior to MTX injection, and blood flow decreased further with MTX injection. At the end of 30 min, concentrations of MTX were significantly higher in the mannitol group compared to the controls: $6 \times 10^{-3} \pm 5 \times 10^{-3}$ versus $2.82 \times 10^{-4} \pm 2.85 \times 10^{-4}$ mg/ml, respectively ($n = 8$, $p < 0.0089$). When compared to the controls, the area under the concentration-time curve was significantly greater in the mannitol group, for both MTX (0.558 ± 0.451 versus 10.66 ± 8.96 mg/ml * s, respectively $n = 8$, $p < 0.007$) and ICG (0.06 ± 0.016 versus 0.179 ± 0.074 mg/ml * s, respectively $n = 8$, $p = 0.006$). Simple linear regression analysis of all 16 animals showed that the end concentration of MTX and the area under the MTX concentration-time curve was related to the ICG concentration observed at the end of 5 min (Fig. 8).

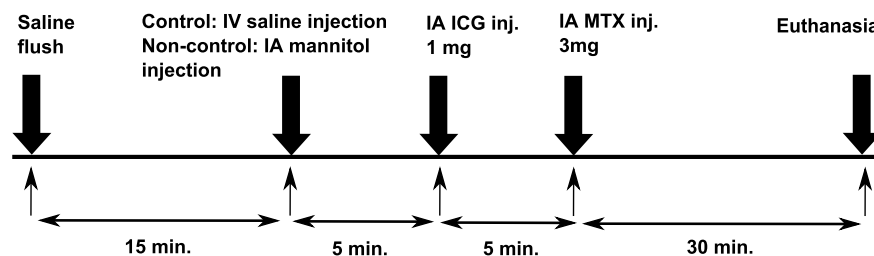


Fig. 6 The experimental protocol (IV: intravenous, IA: intraarterial).

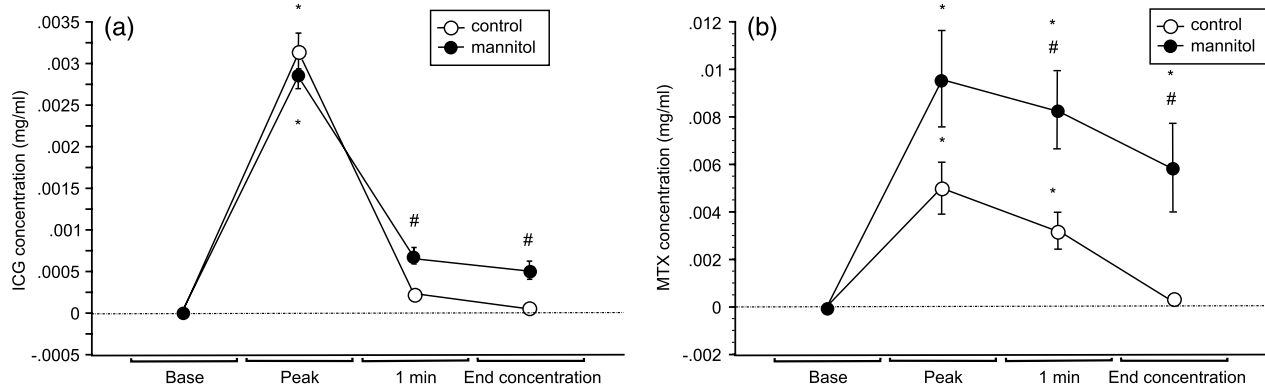


Fig. 7 Changes in tissue concentration of (a) Indocyanine green (ICG) (mg/ml) and (b) Mitoxantrone (MTX) (mg/ml) in control and mannitol-treated animals over time. The figures show mean values with 1-standard error bars. * indicates the statistically significant differences from baseline, and # indicates the statistically significant difference between control and mannitol.

3.2 Physiological Effects of Injection of Mannitol

In this study, mannitol was injected during mild cerebral hypoperfusion, during which the mean arterial pressure was reduced deliberately by injection of adenosine and esmolol to increase the mannitol transit time through the cerebral circulation. There were significant changes in HR, blood pressure, and CBF with mannitol injection, yet the hemodynamic parameters returned to baseline after the injection (Table 1). Due to the hyperemic response after mannitol injection, blood flow data were analyzed with respect to the absolute baseline value for the saline/mannitol run, indicated as %LDF, and the baseline value before each challenge, indicated as $\% \Delta LDF$ in Tables 1–3. CBF changes for injection of mannitol were similar for both of these approaches.

The mixed end-tidal CO_2 value was also recorded in these experiments. This was measured by side stream capnometry, due to the relatively small tidal volume compared to the dead space of the expired gas samples. These values were almost half of those obtained with mainstream end-tidal capnometry on the same animals, but they remained stable throughout the experiment. Oxygen saturation measurements did not reveal any significant changes (Table 1).

3.3 Physiological Effects of IA Injection of ICG

IA injection of ICG resulted in a decrease in CBF flow in both the mannitol and the control groups immediately after injection. A slight but statistically insignificant decrease in MAP was observed during ICG injection. Also, a transient but significant decline in oxygen saturation was seen during ICG injection, both in control and mannitol-treated groups. Other measured parameters showed no significant changes during ICG injection (Table 2).

3.4 Physiological Effects of IA Injection of MTX

Injection of MTX resulted in a transient decrease in CBF and MAP in the mannitol group. Blood flow decreased during MTX injection in the mannitol group and remained low over the next 30 min. 30 min after MTX injection, $\% \Delta LDF$ in the control group was $95 \pm 21\%$ of the challenge baseline value; however, it was $86 \pm 15\%$ ($p < 0.05$) in the mannitol group (Table 3). As in the case of ICG injection, a transient decrease in oxygen saturation was also observed during MTX injection, both in the control and mannitol-treated groups. Other

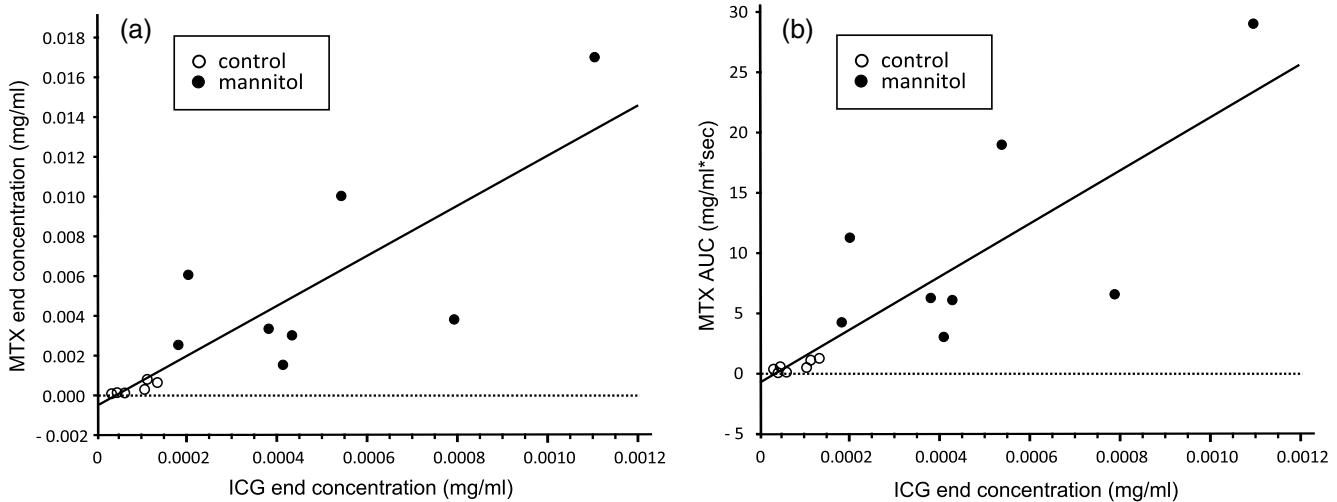


Fig. 8 (a) A correlation was observed between the end ICG (mg/ml) concentrations at the end of 5 min and MTX (mg/ml) concentrations at the end of 30 min ($n = 16$, $R = 0.845$, and $p < 0.0001$). (b) A similar correlation was observed between the end ICG concentrations (mg/ml) and area-under-the MTX concentration-time curve (AUC) (mg/ml * s) ($n = 16$, $R = 0.837$, and $p < 0.0001$).

Table 1 Effect of blood brain barrier disruption: mannitol versus saline.

		Base	Peak	30 s	1 min	5 min
HR (beat/ min)	Control	272 ± 30	272 ± 32 ^a	272 ± 32	270 ± 41	277 ± 33
	Mannitol	266 ± 26	159 ± 66 ^{b,c}	235 ± 66 ^d	265 ± 30 ^d	263 ± 31 ^d
SaO ₂ (%)	Control	97 ± 6	97 ± 6	97 ± 7	97 ± 7	97 ± 7
	Mannitol	100 ± 0	97 ± 4	99 ± 2	100 ± 0	100 ± 0
Mixed ETCO ₂ (mm Hg)	Control	14 ± 3	14 ± 3	14 ± 3	14 ± 3	14 ± 3
	Mannitol	16 ± 3	16 ± 2	16 ± 3	16 ± 3	16 ± 3
Resp. rate (breath/ min)	Control	62 ± 13	62 ± 13	62 ± 13	62 ± 13	62 ± 13
	Mannitol	61 ± 12	61 ± 12	61 ± 12	61 ± 12	61 ± 12
MAP (mmHg)	Control	90 ± 16	87 ± 16 ^a	87 ± 17	87 ± 16	88 ± 16
	Mannitol	85 ± 14	44 ± 29 ^{b,c}	78 ± 32 ^d	92 ± 30 ^d	95 ± 26 ^d
Temperature (°C)	Control	36.2 ± 0.5	36.2 ± 0.5	36.4 ± 0.5	36.5 ± 0.7	36.6 ± 0.7
	Mannitol	36.2 ± 1.2	36.6 ± 1.2	36.5 ± 1.2	36.5 ± 1.3	36.6 ± 1.3
%LDF (saline baseline)	Control	100 ± 0 ^b	95 ± 23 ^a	101 ± 13 ^a	101 ± 12 ^a	104 ± 15 ^a
	Mannitol	100 ± 0	11 ± 13 ^{b,c}	155 ± 37 ^{c,d}	150 ± 53 ^{c,d}	160 ± 60 ^{c,d}
%ΔLDF (challenge baseline)	Control	100 ± 0	95 ± 23 ^a	101 ± 13 ^a	101 ± 12 ^a	104 ± 15 ^a
	Mannitol	100 ± 0 ^b	11 ± 13 ^{b,c}	155 ± 37 ^{c,d}	150 ± 53 ^{c,d}	160 ± 60 ^{c,d}

^aDifferent from mannitol, $p < 0.05$.^bDifferent from 5 min, $p < 0.005$.^cDifferent from base, $p < 0.005$.^dDifferent from peak, $p < 0.005$.**Table 2** Hemodynamic effects of ICG injection.

		Base	Peak	30 s	1 min	5 min
HR (beat/ min)	Control	280 ± 29	268 ± 27	273 ± 25	281 ± 28	281 ± 31
	Mannitol	256 ± 32	251 ± 30	255 ± 28	258 ± 30	264 ± 28
SaO ₂ (%)	Control	95 ± 7 ^b	89 ± 11	93 ± 8	96 ± 6 ^b	96 ± 8 ^b
	Mannitol	99 ± 1 ^b	92 ± 7	99 ± 1 ^b	100 ± 1 ^b	100 ± 0 ^b
Mixed ETCO ₂ (mmHg)	Control	15 ± 3	15 ± 3	15 ± 3	15 ± 3	15 ± 3
	Mannitol	17 ± 3	16 ± 3	16 ± 3	16 ± 3	16 ± 3
Resp. rate (breath/ min)	Control	62 ± 13	62 ± 13	62 ± 13	62 ± 13	62 ± 13
	Mannitol	61 ± 12	61 ± 12	61 ± 12	61 ± 12	61 ± 12
MAP (mmHg)	Control	88 ± 19	78 ± 18	89 ± 25	88 ± 24	86 ± 21
	Mannitol	96 ± 23	85 ± 19	95 ± 18	93 ± 17	89 ± 18
Temperature (°C)	Control	36.6 ± 0.6	36.9 ± 0.6	36.9 ± 0.6	36.7 ± 0.7	36.9 ± 0.7
	Mannitol	36.7 ± 1.3	36.7 ± 1.4	36.8 ± 1.3	36.7 ± 1.3	36.6 ± 1.3
%LDF (saline baseline)	Control	101 ± 10 ^c	43 ± 40 ^{a,d}	92 ± 47	120 ± 28 ^b	123 ± 29 ^b
	Mannitol	139 ± 43	30 ± 37 ^{a,d}	114 ± 40 ^b	118 ± 27 ^b	104 ± 15 ^b
%ΔLDF (challenge baseline)	Control	100 ± 0	44 ± 39 ^{a,d}	91 ± 45 ^b	118 ± 19 ^b	121 ± 20 ^b
	Mannitol	100 ± 0	21 ± 25 ^{a,d}	83 ± 19 ^b	87 ± 11 ^b	79 ± 19 ^b

^aDifferent from 5 min, $p < 0.005$.^bDifferent from peak, $p < 0.005$.^cDifferent from mannitol, $p < 0.05$.^dDifferent from base, $p < 0.005$.

Table 3 Hemodynamic effects of MTX injection.

		Base	Peak	1 min	5 min	30 min
HR (b/ min)	Control	293 ± 20	261 ± 48	265 ± 28	281 ± 25	282 ± 23
	Mannitol	275 ± 35	266 ± 30	265 ± 33	270 ± 30	270 ± 26
SaO ₂ (%)	Control	92 ± 8 ^b	83 ± 13	90 ± 10 ^b	93 ± 8 ^b	91 ± 9 ^b
	Mannitol	100 ± 1 ^b	88 ± 7	95 ± 6	99 ± 1 ^b	100 ± 1 ^b
Mixed ETCO ₂ (mmHg)	Control	15 ± 3	15 ± 2	15 ± 2	15 ± 2	15 ± 2
	Mannitol	16 ± 3	16 ± 3	16 ± 3	16 ± 3	16 ± 3
Resp. rate (breath/ min)	Control	62 ± 13	62 ± 13	62 ± 13	62 ± 13	62 ± 13
	Mannitol	61 ± 12	61 ± 12	61 ± 12	61 ± 12	61 ± 12
MAP (mmHg)	Control	87 ± 17	77 ± 23	86 ± 17	81 ± 16	75 ± 15
	Mannitol	89 ± 16 ^a	73 ± 28 ^c	79 ± 20	74 ± 17 ^c	67 ± 17 ^c
Temperature (°C)	Control	36.8 ± 0.9	36.9 ± 0.9	36.8 ± 1.0	37.4 ± 1.3	37 ± 1.5
	Mannitol	36.6 ± 1.4	36.6 ± 1.4	36.5 ± 1.4	36.6 ± 1.6	36.6 ± 1.8
%LDF (saline baseline)	Control	107 ± 21	92 ± 26	100 ± 9	103 ± 1 ^d	100 ± 19
	Mannitol	99 ± 16 ^b	55 ± 43	97 ± 14 ^b	83 ± 16	86 ± 21
%ΔLDF (challenge baseline)	Control	100 ± 0	87 ± 28	95 ± 15	98 ± 18 ^d	95 ± 21 ^d
	Mannitol	100 ± 0 ^b	56 ± 44	99 ± 11 ^b	85 ± 14	86 ± 15

^aDifferent from 5 min, $p < 0.005$.

^bDifferent from peak, $p < 0.005$.

^cDifferent from base, $p < 0.005$.

^dDifferent from mannitol, $p < 0.05$.

hemodynamic parameters remained stable during the MTX injection (Table 3).

4 Discussion

One of the important findings of this study is that, although variable, the disruption of the BBB with mannitol, compared to the controls, significantly increases tissue ICG concentrations 5 min after an IA injection of mannitol. Disruption of the BBB also significantly increases the uptake of IA MTX, and the uptake of MTX is correlated to the tissue ICG concentrations determined just prior to MTX injection.

In this study, we used IA injection of ICG to assess BBB and rapidly detect any tissue uptake. There are conflicting data regarding the uptake of ICG after BBB, even though ICG is retained both by tumor tissue and in the infarcted regions of the brain where the barrier functions are impaired.^{24,25} In this study, supporting the use of the OP method with ICG as a marker for BBB, we found that there was a significant difference in ICG concentration at 5 min between the mannitol and the control groups.

We also observed a decrease in CBF during ICG injection. A transient decline in oxygen saturation was also noted during ICG and MTX injections. This is likely due to the effect of displacement of blood by the drug. LD measurements are based on the concentration and velocity of red blood cells. Any dilution of the red cells would translate into a decrease in measured blood

flow. Without another method to measure CBF that is not affected by dilution, it is difficult to assess the effect of ICG on CBF. Further studies will be undertaken to resolve this issue. In contrast to bolus ICG injection, which generated comparable peak concentrations in mannitol and control groups, infusion of MTX over 30 s generated different peak concentrations in those groups. This difference could reflect differences in the blood flow state in the two groups compared to baseline. IA infusion of MTX produced a less profound decrease in CBF in the control group. Injection of MTX in the control group resulted in a relatively smaller decrease in LDF values: 92 ± 26% in the control group versus 55 ± 43% in the mannitol group ($p = 0.057$). Although the difference did not achieve statistical significance, such a decrease in blood flow could explain the relatively higher peak concentrations of MTX in the mannitol group.

The key result of this study, however, is not the uptake of ICG or MTX, but the correlation that was observed between the end concentrations of ICG and the end concentrations of MTX and its area under the concentration-time curve, as shown in Fig. 8. With the control and the mannitol groups combined, the MTX concentrations at the end of 30 min were directly related to the ICG concentration at the end of 5 min ($n = 16$, $R = 0.845$, $p < 0.0001$). A similar value ($n = 16$, $R = 0.837$, $p < 0.0001$) was obtained for area under the MTX concentration-time curve.

Prior to discussing the significance of this observation, one has to see the potential weaknesses. The OP method determines the total tissue concentration of drugs, irrespective of whether the drug is contained in the vascular or extra-vascular space within the interrogated tissue. In most healthy tissue, the blood compartment is a small component (3% to 5%) of the tissue mass. If a drug has a blood:tissue partition coefficient of 1, then the OP signal from the blood has a small contribution. However, if the blood:tissue partition coefficient is low, then OP measured tissue uptakes can be profoundly affected by changes in CBF. Any bleeding into the tissue or even a hyperemic response could increase the measured tissue concentrations of drug. Significant bleeding under the probe site is easily detected by strong hemoglobin absorption around 550 nm and can be remedied by irrigating the probe site. However, flushing will not be able to correct for bleeding within the cranial vault or for a hyperemic response.

In addition, it should be noted that a decrease in blood flow during IA injection of a drug will increase the drug's concentration by decreasing the dilution with blood. The peak concentration of a drug after an IA injection is a function of blood flow and the volume rate of injection. When there is an excess volume of drug injection, as in the case of ICG, the peak concentrations are very reproducible as the dead space of the vasculature (the vascular density of the tissue and its potential to dilate) is relatively small compared to the large volume of the injection. However, this relationship becomes more complex and less predictable as the rate of injection relative to blood flow decreases. The peak concentrations will vary greatly when IA drug infusion rates are relatively small compared to blood flow, as was the case with MTX. We are presently evaluating the possibility of using short saline flushes that momentarily displace all blood in the interrogated tissue to determine tissue concentrations. In this study, this correction was only applied to calculate the peak ICG and MTX concentrations.

This study underscores the need to develop optical methods to assess BBBD in real time to improve IA chemotherapy. Although ICG appears to be a suitable marker for BBBD, further studies are warranted to develop human applications, in light of the observed effects of ICG on the CBF. The intravenous ICG clearance curve has been used at bedside to measure CBF in human patients using near-infrared spectroscopy.^{26,27} The short half-life of ICG, its long track record of safe human use, and the possibility of developing optical methods based on absorption and fluorescent techniques to assess its tissue concentrations encouraged us to evaluate ICG as the tracer.²⁸ If ICG is to be used for the assessment of BBBD in humans, its formulation will have to be optimized to address safety issues, particularly for IA injections.

In conclusion, this study found that the uptake of MTX was significantly increased after BBBD and was correlated to the ICG concentrations 5 min after IA injection of the tracer and prior to the injection of MTX. Further investigations are necessary to improve this technology such that, eventually, optically assessed BBB permeability will help in optimizing the dose of mannitol, adjust the dose of chemotherapeutic drugs, and possibly prevent complications arising from excessive BBBD.

Acknowledgments

This work was supported in part by the National Cancer Institute R01 (R01-CA-12500, and CA-138643, SJ, and R01-CA82104; U54-CA104677, IB).

References

1. E. Neuwelt et al., "Strategies to advance translational research into brain barriers," *Lancet Neurol.* **7**(1), 84–96 (2008).
2. M. A. Bellavance, M. Blanchette, and D. Fortin, "Recent advances in blood-brain barrier disruption as a CNS delivery strategy," *AAPS J.* **10**(1), 166–177 (2008).
3. S. Joshi, P. M. Meyers, and E. Ornstein, "Intraarterial delivery of drugs: the potential and the pitfalls," *Anesthesiology* **109**(3), 543–564 (2008).
4. R. L. Dedrick, "Arterial drug infusion: pharmacokinetic problems and pitfalls," *J. Natl. Canc. Inst.* **80**(2), 84–89 (1988).
5. I. J. Bigio, J. R. Mourant, and G. Los, "Noninvasive, in-situ measurement of drug concentrations in tissue using optical spectroscopy," *J. Gravit. Physiol.* **6**(1), 173–175 (1999).
6. J. R. Mourant et al., "Non-invasive measurement of chemotherapy drug concentrations in tissue: preliminary demonstrations of *in vivo* measurements," *Phys. Med. Biol.* **44**(5), 1397–1417 (1999).
7. R. Reif et al., "Optical method for real-time monitoring of drug concentrations facilitates the development of novel methods for drug delivery to brain tissue," *J. Biomed. Opt.* **12**(3), 034036 (2007).
8. S. Joshi et al., "Intra-arterial mitoxantrone delivery in rabbits: an optical pharmacokinetic study," *Neurosurgery* **69**(3), 706–712 (2011).
9. S. C. Kanick et al., "Noninvasive and nondestructive optical spectroscopic measurement of motexafin gadolinium in mouse tissues: comparison to high-performance liquid chromatography," *J. Photochem. Photobiol.* **88**(2–3), 90–104 (2007).
10. S. Joshi et al., "Use of intravenous indocyanine green as a marker of blood brain barrier disruption (abstracts)," *J. Neurosurg. Anesthesiol.* **22**(4), 433–434 (2010).
11. M. Wang, J. Etu, and S. Joshi, "Enhanced disruption of the blood brain barrier by intraarterial mannitol injection during transient cerebral hypoperfusion in rabbits," *J. Neurosurg. Anesthesiol.* **19**(4), 249–256 (2007).
12. S. Joshi et al., "Inconsistent blood brain barrier disruption by intraarterial mannitol in rabbits: Implications for chemotherapy," *J. Neurooncol.* **104**(1), 11–19 (2010).
13. E. Zylber-Katz et al., "Pharmacokinetics of methotrexate in cerebrospinal fluid and serum after osmotic blood-brain barrier disruption in patients with brain lymphoma," *Clin. Pharmacol. Ther.* **67**(6), 631–641 (2000).
14. N. Marchi et al., "Seizure-promoting effect of blood-brain barrier disruption," *Epilepsia* **48**(4), 732–742 (2007).
15. F. Rebeles, "Blood-brain barrier imaging and therapeutic potentials," *Top. Magn. Reson. Imaging* **17**(2), 107–116 (2006).
16. B. Zunkeler et al., "Quantification and pharmacokinetics of blood-brain barrier disruption in humans," *J. Neurosurg.* **85**(6), 1056–1065 (1996).
17. J. R. Mourant et al., "Measuring absorption coefficients in small volumes of highly scattering media: source-detector separations for which path lengths do not depend on scattering properties," *Appl. Opt.* **36**(22), 5655–5661 (1997).
18. I. J. Bigio and S. G. Bown, "Spectroscopic sensing of cancer and cancer therapy: current status of translational research," *Cancer Biol. Ther.* **3**(3), 259–267 (2004).
19. M. L. Landsman et al., "Light-absorbing properties, stability, and spectral stabilization of indocyanine green," *J. Appl. Physiol.* **40**(4), 575–583 (1976).
20. S. Prahl, "Optical Absorption of Indocyanine Green (ICG)," Oregon Medical Laser Center, <http://omlc.ogi.edu/spectra/icg/index.html> (July 5 2011).
21. B. S. Lee and P. K. Dutta, "Optical spectroscopic studies of the anti-tumor drug 1,4-dihydroxy-5,8-bis[2-[(2-hydroxyethyl)amino]ethyl]amino]-9,10-anthracenedione (mitoxantrone)," *J. Phys. Chem.* **93**(15), 5665–5672 (1989).
22. S. Joshi, M. Wang, and R. Hartl, "Retinal discoloration test," *J. Cereb. Blood Flow Metab.* **24**(3), 305–308 (2004).
23. V. Rousseau et al., "Investigation of blood-brain barrier permeability to magnetite-dextran nanoparticles (MD3) after osmotic disruption in rats," *Magma* **5**(3), 213–222 (1997).
24. D. E. Kim et al., "Near-infrared fluorescent imaging of cerebral thrombi and blood-brain barrier disruption in a mouse model of cerebral venous

- sinus thrombosis," *J. Cereb. Blood Flow Metab.* **25**(2), 226–233 (2005).
25. M. Kala, "Indocyanine green (ICG) staining and demarcation of tumor margins in a rat glioma model," *Surg. Neurol.* **42**(6), 552–554 (1994).
26. E. Keller et al., "Noninvasive measurement of regional cerebral blood flow and regional cerebral blood volume by near-infrared spectroscopy and indocyanine green dye dilution," *Neuroimage* **20**(2), 828–839 (2003).
27. M. Kohl-Bareis et al., "Noninvasive monitoring of cerebral blood flow by a dye bolus method: separation of brain from skin and skull signals," *J. Biomed. Opt.* **7**(3), 464–470 (2002).
28. J. Steinbrink et al., "Towards noninvasive molecular fluorescence imaging of the human brain," *Neurodegener. Dis.* **5**(5), 296–303 (2008).